NASA Contractor Report 191503

ICASE Report No. 93-45

AD-A271 853
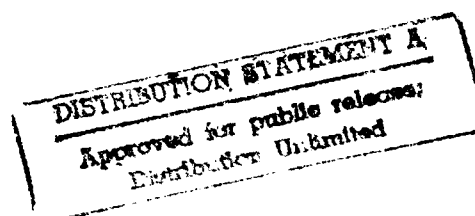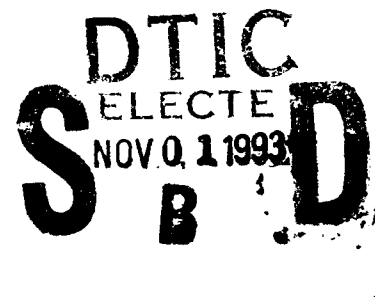
ICASE

20 Years of Excellence

ANALYTICAL DESCRIPTION OF THE BREAKUP
OF LIQUID JETS IN AIR

DTIC
ELECTE
NOV 0 1 1993
S
B
D

Demetrios T. Papageorgiou

93-25867

National Aeronautics and
Space Administration

Langley Research Center
Hampton, Virginia 23681-0001

93 10

ICASE Fluid Mechanics

Due to increasing research being conducted at ICASE in the field of fluid mechanics, future ICASE reports in this area of research will be printed with a green cover. Applied and numerical mathematics reports will have the familiar blue cover, while computer science reports will have yellow covers. In all other aspects the reports will remain the same; in particular, they will continue to be submitted to the appropriate journals or conferences for formal publication.

ANALYTICAL DESCRIPTION OF THE BREAKUP OF LIQUID JETS IN AIR

Demetrios T. Papageorgiou[1]
Department of Mathematics and
Center for Applied Mathematics and Statistics
New Jersey Institute of Technology
Newark, New Jersey 07102

ABSTRACT

A viscous or inviscid cylindrical jet with surface tension in a vacuum tends to pinch due to the mechanism of capillary instability. We construct similarity solutions which describe this phenomenon as a critical time is encountered, for two physically distinct cases: (i) Inviscid jets governed by the Euler equations, (ii) highly viscous jets governed by the Stokes equations. In both cases the only assumption imposed is that at the time of pinching the jet shape has a radial length scale which is smaller than the axial length scale. For the inviscid case, we show that our solution corresponds exactly to one member of the one-parameter family of solutions obtained from slender jet theories and the shape of the jet is locally concave at breakup. For highly viscous jets our theory predicts local shapes which are monotonic increasing or decreasing indicating the formation of a mother drop connected to the jet by a thin fluid tube. This qualitative behavior is in complete agreement with both direct numerical simulations and experimental observations.

iii

1 Introduction

It is well known (Rayleigh (1878)), that a circular jet of finite radius with a surface which supports surface tension is linearly unstable to a long-wave capillary instability. Any small perturbations with wavelengths larger than the jet radius grow exponentially. Furthermore, linear theory predicts a maximally growing wave and hence a dominant length scale for the instability. According to linear theory, then, the dominant wavelength is approximately $9a$ where a is the unperturbed jet radius (this result is independent of the surface tension coefficient). Experiments indicate that the instability can lead to breakup, or pinching, of the jet into drops. Clearly the pinching phenomenon is nonlinear since the initial disturbance has to grow to amplitudes of the order of the unperturbed jet radius. Linear theory, however, does well in the qualitative prediction of breakup times, for instance, by employment of empirical arguments such as e-fold amplification of perturbations. In many applications the shape and jet velocities at breakup are useful but cannot be obtained from linear theory. This classical problem has been studied extensively; experiments have been carried out by Donnelly and Glaberson (1966), Goedde and Yuen (1970) and more recently Chaudhary and Maxworthy (1980a,b). Weakly nonlinear theories (see below) have been carried out by Yuen (1968) and later by Chaudhary and Redekopp (1980). A review of the subject can be found in Bogy (1979) while recent simulations using boundary integral techniques are described in Mansour and Lundgren (1990).

Viscosity dominated flows form a separate but parallel field. Tomotika (1936) considered the linear stability of a stationary cylindrical thread of viscous fluid surrounded by a second viscous fluid with surface tension acting at the interface. Qualitatively, the stability results are similar to inviscid studies with a maximally growing wave of the order of the unperturbed thread radius. A more complete theory, including the effects of non-uniform jet velocities can be found in Chandrasekhar (1961), where it is shown that capillary instability provides linearly growing waves that scale on the jet radius. Recently, Tjahjadi, Stone and Ottino (1992), have undertaken an experimental and numerical study of breakup of viscous cylindrical threads of one fluid in another. The experiments and the computations show that at the time of breakup the jet tends to form larger mother drops joined to smaller satellite drops by thin slender tubes. It is precisely this regime that we can describe theoretically with excellent qualitative agreement with both computations and experiments. Besides their intrinsic interest, such solutions can be useful in providing initial conditions for continuation of numerical solutions just before the change in topology necessitated by the pinching. The analytical description of local structures is also useful in the determination of the effect of additional physicochemical effects such as surface active agents or electrical forces on the

1

pinching process.

The present approach is a fully nonlinear one with interfacial deflections as large as the undisturbed jet radius, as opposed to most previous weakly nonlinear studies. Chaudhary and Redekopp (1980) (see also Yuen (1968)) consider two low amplitude (asymptotically small but not infinitesimally so) initial perturbations, a fundamental and a harmonic. These are followed up to cubic order in the initial small amplitude, which is the first stage when the modes interact nonlinearly to produce an amplitude equation. The methodology is that of the Stuart (1960), Watson (1960) classical weakly nonlinear theory, even though the jet problem always has a band of unstable waves which does not become monochromatic as a flow parameter (e.g. capillary number here) is varied. The results are therefore expected to be valid for sufficiently small times, but as Chaudhary and Redekopp indicate qualitative features of the experiments are reproduced at times which seem to be beyond the validity of the theory. Fully nonlinear theories allow the interfacial amplitude to be as large as the unperturbed jet radius, a situation which is essential in the description of breakup. This usually means that the problem should be addressed numerically, and it is the objective of this work to present an analytical alternative to breakup. A fully nonlinear theory of jet breakup in a vacuum was developed by Ting and Keller (1991), referred to as TK. This is done by use of slender jet theory (see below) which was extended by Papageorgiou and Orellana (1993), referred to as PO, to describe breakup of jets of one fluid into another with different density, with or without surface tension and inclusion of Kelvin-Helmholtz instability. In both cases, a simplified set of evolution equations involving time and the axial coordinate alone, are derived by an asymptotic expansion procedure which uses the ratio between undisturbed jet radius to characteristic axial length scale as a small parameter. As noted by Papageorgiou and Orellana, such an ansatz can be applied to flows which have initial conditions characterized by a long axial length scale, for instance. This implies that the slender jet theory preserves such geometry throughout the evolution and at the time of pinching the distance between successive pinch points is large compared to the undisturbed jet radius. Qualitatively, therefore, the slender jet theory predicts drops with radii larger than the undisturbed jet radius. The strength of the slender jet theory, however, is in its prediction of local structures at the time of pinching. As found in TK and extended to other flows by PO, a one-parameter family of similarity solutions is possible. Different members of this family correspond to local geometrical shapes of the jet which are concave, conical and convex respectively (see PO for representative numerical solutions). In this work we show that if the slender jet theory is not adopted throughout the evolution, the jet can pinch according to a single member of the one-parameter slender jet family, corresponding to concave shapes. Solutions with zero surface tension also follow by simply discarding one

2

term from the similarity equations. As shown in PO, the slender jet equations with zero surface tension constitute a system of two nonlinear hyperbolic conservation laws with the final outcome of the initial value problem being the formation of a shock after a finite time. Clearly the development of short axial length scales is inconsistent with the fundamental assumptions of the theory. The direct theory presented here, however, does not assume the slender jet approximation *throughout* the evolution and so does not suffer from the restrictions outlined above. Consequently, a pinching solution for zero surface tension can be given for a flow which is stable according to linear theory. The shapes at breakup are monotonic indicating the possibility of formation of mother drops joined to satellite drops by thin fluid tubes. Such shapes are seen in experimental studies of inviscid jets (see Donnelly and Glaberson (1966)).

We emphasize that slender jet theories are powerful methods in the description of local structures in pinching phenomena. In capillary instability phenomena in three dimensions, slender jet theories provide simplified sets of evolution equations which can be analyzed for breakup. Since at breakup of cylindrical jets the slender jet assumptions are valid it is not surprising to find that a description of breakup emerges. Physically, the disturbance must be characterized by large wavelengths initially. The present approach corresponds to a different physical set-up as we describe next. If the jet is allowed to undergo natural growth without any external forcings and linear waves are at first important, then linear theory can be used to predict a maximally growing wave. As mentioned above, this wave has wavelength of the order of the undisturbed jet radius and so when the evolution enters the nonlinear regime, the interfacial waves have axial length scales comparable to the undisturbed jet radius. The slender jet approximation may not be appropriate, therefore, for the *total* duration of the evolution to breakup, even though it is appropriate locally at breakup. The analysis presented here, assumes that near the singular time the jet radius is asymptotically smaller than the axial length scale, a condition which may be inappropriate for the past history of the evolution.

The article is organized as follows. Section 2 deals with the breakup of inviscid jets governed by the axially symmetric Euler equations. A system of differential equations is derived that describes the local structure of the shape and the potential of the jet at breakup. Numerical solutions are given and a correspondence is made with the slender jet results of PO, both in the presence and absence of surface tension. In Section 3 we analyze viscous axisymmetric jets. The equations studied are the Stokes equations (creeping motion corresponding to small Reynolds numbers) and a differential equation describing the jet shape at breakup emerges. The analysis leading to this equation is more involved than the inviscid case due to the higher order of the field equation and the additional stress boundary condi-

3

tions. Numerical and analytical aspects of the equation are also given. Finally Section 4 is devoted to discussion and comparison with experiments and simulations.

2 The theory for inviscid jets

The equations governing the fluid motion can be written in terms of a velocity potential $\phi(t, r, z)$ which is independent of the azimuthal angle θ for axisymmetric flows. A system of cylindrical polar coordinates (r, θ, z) is used with corresponding velocity vector $\mathbf{u} = (u, v, w) = \nabla \phi$. Using this notation, ϕ satisfies Laplace's equation while at the free surface two conditions are specified, a kinematic condition and a normal stresses balance which gives the pressure jump across the interface. When the latter condition is used in the z-momentum equation the usual Bernoulli equation arises. Without loss of generality we give the system for a static undisturbed jet, noting that any background axial velocity can be removed by a Galilean transformation. The equations with boundary conditions are

$$\phi_{rr} + \frac{1}{r}\phi_r + \phi_{zz} = 0, \tag{2.1a}$$

On $r = S(t, z)$,

$$\phi_r = S_t + \phi_z S_z, \tag{2.1b}$$

$$\phi_t + \frac{1}{2}(\phi_r^2 + \phi_z^2) = -\left(\frac{1}{S} - S_{zz} + \frac{S_z^2 S_{zz}}{1 + S_z^2}\right)(1 + S_z^2)^{-1/2}. \tag{2.1c}$$

A final condition which completely specifies the problem is regularity of ϕ at $r = 0$. Equations (2.1a-c) are in non-dimensional form with the non-dimensional group containing the surface tension coefficient (the Weber number) scaled to unity, in anticipation of this canonical rescaling in the final similarity equations.

In general (2.1a-c) must be addressed numerically. We construct pinching solutions of (2.1a-c) by assuming the following ansatz as a singular time t_s is approached from below:

$$r = (t_s - t)^\alpha y \quad , \quad z = (t_s - t)^\beta \xi \quad , \quad S(t, z) = (t_s - t)^\alpha f(\xi), \tag{2.2a}$$

$$\phi(t, r, z) = (t_s - t)^\gamma \chi(t, y, \xi). \tag{2.2b}$$

According to these transformations time and space derivatives become

$$\frac{\partial}{\partial t} \to \frac{\partial}{\partial t} + \frac{\beta \xi}{(t_s - t)} \frac{\partial}{\partial \xi},$$

$$\frac{\partial}{\partial r} \to (t_s - t)^{-\alpha} \frac{\partial}{\partial y} \qquad \frac{\partial}{\partial z} \to (t_s - t)^{-\beta} \frac{\partial}{\partial \xi}. \tag{2.2c}$$

4

Physically, we expect the jet radius to be much smaller than the axial length scale at breakup. This implies that $r \ll z$ which in turn yields the condition

$$\alpha > \beta. \tag{2.3}$$

Inequality (2.3) is the only necessary assumption for the theory to be consistent.

Substitution of the ansatz (2.2a-c) into the Laplace equation (2.1a) indicates that since $\alpha > \beta$, the dominant terms come from the r-derivatives. The leading order contribution which is regular at the jet axis $y = 0$ is independent of y, and we must go to a higher order to obtain a non-trivial balance. This suggests seeking a solution by expanding χ in (2.2b) in appropriate powers of $(t_s - t)$ as follows:

$$\phi = (t_s - t)^\gamma \left(\chi_0(y,\xi) + (t_s - t)^\beta \chi_1(y,\xi) + (t_s - t)^\alpha \chi_2(y,\xi) + \ldots \right). \tag{2.4}$$

Substitution of (2.4) into the Laplace equation (2.1a) gives

$$(t_s - t)^{\gamma - 2\alpha} \left(\chi_{0yy} + \frac{1}{y}\chi_{0y} \right) + (t_s - t)^{\gamma + \beta - 2\alpha} \left(\chi_{1yy} + \frac{1}{y}\chi_{1y} \right) +$$

$$(t_s - t)^{\gamma - 2\beta} \chi_{0\xi\xi} + \ldots = 0. \tag{2.5}$$

It can be seen from (2.5) that the first stage where a regular y-dependent solution is possible, arises if the χ_1 terms are in balance with the $\chi_{0\xi\xi}$ term. This yields

$$\alpha = \frac{3}{2}\beta. \tag{2.6}$$

The solutions for χ_0 and χ_1 which are regular at $y = 0$ are

$$\chi_0 = A(\xi), \qquad \chi_1 = -\frac{1}{4}y^2 A_{\xi\xi} + B(\xi), \tag{2.7a, b}$$

where A and B are unknown functions of ξ.

Next we consider the kinematic condition (2.1b). Substitution of the ansatz (2.2) and (2.4) along with the solutions (2.7a,b) yields the equation

$$(t_s - t)^{\gamma + \beta - \alpha} \left(-\frac{1}{2}f A_{\xi\xi} \right) = -\alpha(t_s - t)^{\alpha - 1} f$$

$$+ \beta(t_s - t)^{\alpha - 1} \xi f_\xi + (t_s - t)^{\gamma + \alpha - 2\beta} A_\xi f_\xi + \ldots \quad . \tag{2.8}$$

A few comments about (2.8) are in order. First, the two terms which contain A are multiplied by the powers $\gamma + \beta - \alpha$ and $\gamma + \alpha - 2\beta$ of $(t_s - t)$ respectively. Since $\alpha = \frac{3}{2}\beta$ from (2.6) these terms are in balance and provide no new information. An expression for γ is next found by making a balance of all four leading order terms in (2.8). This gives

$$\gamma = 2\beta - 1, \tag{2.9}$$

5

and the kinematic condition becomes to leading order

$$-\frac{1}{2}fA'' = -\frac{3}{2}\beta f + \beta\xi f' + f'A', \qquad (2.10)$$

where primes denote ξ-derivatives.

Another equation, as well as determination of the free parameter β is found from the Bernoulli equation (2 1c). Substitution of the ansatz (2.2), (2.4) and retention of the largest possible terms as $t \to t_s-$, gives the following equation:

$$-\gamma(t_s - t)^{\gamma-1}A + (t_s - t)^{\gamma-1}\beta\xi A_\xi + (t_s - t)^{2\gamma-2\beta}\frac{1}{2}A_\xi^2 = -(t_s - t)^{-\alpha}f^{-1}. \qquad (2.11)$$

We arrive at (2.11) above by dropping any terms that are smaller than the ones retained using the fact that $\alpha > \beta$ alone. Next, we balance the different terms in the equation. The terms of orders $(t_s - t)^{\gamma-1}$ and $(t_s - t)^{2\gamma-2\beta}$ are in balance by virtue of (2.9) above. The surface tension term containing f^{-1} is chosen to balance the other terms and produces a coupling with (2.10) between inertial and capillary forces. This is possible if

$$\gamma - 1 = -\alpha.$$

Use of (2.6) and (2.9) that provide α and γ in terms of β yields a value for β and hence α and γ follow,

$$\alpha = \frac{6}{7} \quad , \quad \beta = \frac{4}{7} \quad , \quad \gamma = \frac{1}{7}, \qquad (2.12)$$

while equation (2.11) becomes

$$-\frac{1}{7}A + \frac{4}{7}\xi A_\xi + \frac{1}{2}A_\xi^2 = -\frac{1}{f}. \qquad (2.13)$$

Equations (2.10) and (2.13) form a coupled system which must in general be addressed numerically. Before presentation of such results we cast (2.10), (2.13) into a form which is readily comparable with the one-parameter family equations of PO. We define $G = A_\xi$ and $f = \sqrt{F}$, differentiate (2.13) with respect to ξ to yield the system

$$-\frac{12}{7}F + \frac{4}{7}\xi F' + (GF)' = 0, \qquad (2.14a)$$

$$\frac{3}{7}G + \frac{4}{7}\xi G' + \frac{1}{2}(G^2)' = -(F^{-1/2})'. \qquad (2.14b)$$

Equations (2.14a,b) are exactly the equations found from slender jet theory corresponding to $\beta = \frac{4}{7}$. In the absence of surface tension the term on the right hand side of (2.14b) is dropped. As shown below, zero surface tension solutions are possible even though the flow is

linearly stable. Before presentation of numerical solutions we give the asymptotic behavior of (2.14a,b) for large $|\xi|$ (for more details see PO). In the absence of surface tension we find

$$F \sim \xi^3 \quad G \sim \xi^{-\frac{3}{4}} \quad \xi \to \infty, \tag{2.15a}$$

$$F \sim (-\xi)^{-1} \quad G = -\xi + \ldots \quad \xi \to -\infty. \tag{2.15b}$$

Note that the shapes predicted for zero surface tension grow on one side (as $\xi \to \infty$ here) and decay at the other end of the domain. This is in contrast to the surface tension case as the following asymptotic forms indicate,

$$F \sim \xi^3 \quad G \sim \xi^{-\frac{3}{4}} \quad \xi \to \infty, \tag{2.16a}$$

$$F \sim (-\xi)^3 \quad G \sim (-\xi)^{-\frac{3}{4}} \quad \xi \to -\infty. \tag{2.16b}$$

Numerical solutions of (2.14a,b) showing the variation of F and G with ξ are given in Figures 1 and 2 for zero surface tension. Verification of the asymptotic forms (2.15a,b) is included in Figures 3 and 4 for the behavior of F and G respectively. This is achieved by constructing logarithmic plots of the numerical solutions for large positive and negative ξ. The slopes of the lines so obtained were computed from the data by a least squares fit and are indicated on the Figures. It is seen that agreement is very good and improves as the range of integration is extended. The results for non-zero surface tension are presented in Figures 5 and 6 with the corresponding logarithmic plots confirming the asymptotic behavior in Figures 7 and 8. The main qualitative difference between the two cases is that in the absence of surface tension the shape is monotonic tending to zero at one end of the similarity region and growing algebraically at the other end, while in the presence of surface tension the shape function grows algebraically (at the same asymptotic rate) at both ends of the domain. The former type of behavior is also obtained for highly viscous jets analyzed in Section 3.

2.1 Conservation integrals at breakup.

The inviscid jet flow is conservative and solutions to the problem are required to conserve the total momentum and energy as well as mass. It can be seen from the solutions just constructed that velocities are becoming unbounded as the jet radius shrinks to zero. It is important, therefore, to verify the consistency of these solutions with conserved quantities of the system. We define the total mass, momentum and energy of an axially periodic portion of the jet by I_1, I_2 and I_3 respectively. These are given by

$$I_1 = 2\pi\rho \int_{-D}^{D} \int_0^S r\,dr\,dz, \tag{2.17}$$

7

$$I_2 = 2\pi\rho \int_{-D}^{D} \int_{0}^{S} (\phi_r^2 + \phi_z^2)^{1/2} r\,dr\,dz, \tag{2.18}$$

$$I_3 = 2\pi\rho \int_{-D}^{D} \int_{0}^{S} \frac{1}{2} (\phi_r^2 + \phi_z^2) r\,dr\,dz + 2\pi\sigma \int_{-D}^{D} S\,dz, \tag{2.18}$$

where σ is the surface tension co·''ient and the quantities (2.17)-(2.19) are in dimensional forms. The contributions of the integrals I_1, I_2 and I_3 in the similarity region are found by substitution of the leading order solutions from the ansatz (2.2a-c) to give the following quantities

$$I_1 \sim (t_s - t)^{\frac{16}{7}} \int_{-\infty}^{\infty} F\,d\xi, \tag{2.19}$$

$$I_2 \sim (t_s - t)^{\frac{13}{7}} \int_{-\infty}^{\infty} FG\,d\xi. \tag{2.20}$$

$$I_3 \sim (t_s - t)^{\frac{10}{7}} \int_{-\infty}^{\infty} FG^2\,d\xi. \tag{2.21}$$

The contributions to the energy integral (2.18) of the kinetic and surface energy in the similarity region are of the same order and form and both appear in (2.21); the expression, therefore, is valid both in the absence and presence of surface tension. We have shown analytically and numerically that F and G become unbounded as $|\xi| \to \infty$. In order to evaluate the contributions (2.19)-(2.21) on the large scale flow we need to transform to outer variables. The main contributions to the integrals come from the asymptotic forms (2.15a,b) for zero surface tension or (2.16a,b) for non-zero tension. The behavior at infinity, however, is the same for both cases and the results that follow are equally valid. Consideration of the leading order contributions of (2.19)-(2.21) gives

$$I_1 \sim (t_s - t)^{\frac{16}{7}} \xi^4 = z^4, \tag{2.22}$$

$$I_2 \sim (t_s - t)^{\frac{13}{7}} \xi^{\frac{13}{7}} = (t_s - t)^{\frac{39}{49}} z^{\frac{13}{7}}, \tag{2.23}$$

$$I_3 \sim (t_s - t)^{\frac{10}{7}} \xi^{\frac{5}{2}} = z^{\frac{5}{2}}. \tag{2.24}$$

We can conclude from (2.22)-(2.24) that as the singular time is approached, the solutions constructed here are consistent with the conservation integrals of the problem. More specifically the total mass, momentum and energy in the breakup region tends to zero as the singular time is reached. This theoretical result can be of used as a criterion in numerical simulations, for example, since near the singular time the total energy of the system is concentrated away from the similarity region.

3 Theory for viscous jets

In this section we consider the collapse of a viscous thread of fluid of undisturbed radius R under capillary instability. In numerous applications characteristic Reynolds numbers are

small and the flow is governed by the Stokes equations. Such flows are driven by capillary forces which in turn provide a scale for the flow velocities. In non-dimensionalizing the equations, therefore, the following scales are used:

$$(r, z) = R(\bar{r}, \bar{z}) \quad (u, w) = \frac{\sigma}{\mu}(\bar{u}, \bar{w}) \quad p = \frac{\sigma}{R}\bar{p} \quad t = \frac{\mu R}{\sigma}\bar{t},$$

where σ is the surface tension coefficient and μ the fluid viscosity. The non-dimensional equations and interfacial boundary conditions become (dropping the bars):

$$\triangle u - \frac{1}{r^2}u = p_r, \tag{3.1a}$$

$$\triangle w = p_z, \tag{3.1b}$$

$$\frac{1}{r}(ru)_r + w_z = 0, \tag{3.1c}$$

$$\triangle \equiv \frac{\partial^2}{\partial r^2} + \frac{1}{r}\frac{\partial}{\partial r} + \frac{\partial^2}{\partial z^2}.$$

On $r = S(t, z)$ we have

$$(u_z + w_r)(1 - S_z^2) + 2u_r S_z - 2w_z S_z = 0, \tag{3.1d}$$

$$p - 2u_r - (-p + 2w_z)S_z^2 + 2(u_z + w_r)S_z =$$

$$-\left(S_{zz} - \frac{1}{S}(1 + S_z^2)\right)(1 + S_z^2)^{-1/2}, \tag{3.1e}$$

$$u = S_t + wS_z. \tag{3.1f}$$

The interfacial conditions (3.1d-f) represent the tangential stress balance, normal stress balance and the kinematic condition respectively. An additional condition is regularity of the velocity field on the jet axis $r = 0$. The problem (3.1a-f) poses a formidable analytical task. Analytical studies are usually confined to linear stability and in the fully nonlinear regime the problem has been addressed numerically (see Introduction). In order to draw up an analogy with the inviscid analysis of Section 2, we can introduce a streamfunction ψ defined by $u = -\frac{1}{r}\psi_z$, $w = \frac{1}{r}\psi_r$ so that the continuity equation (3.1c) is satisfied. Elimination of p between (3.1a,b) yields a single equation for ψ, namely

$$E^4\psi = 0, \qquad E^2 \equiv \triangle - \frac{2}{r}\frac{\partial}{\partial r}. \tag{3.2}$$

The flow field in the viscous case is governed by a fourth order equation as opposed to the second order Laplace equation for the potential in inviscid flows. As seen below the analysis of viscous jet pinching is slightly more involved. In what follows we choose to work with primitive variables rather than with the streamfunction ψ.

9

Following the ideas developed in Section 2, we look for singular terminal states of (3.1a-f) according to the ansatz

$$r = (t_s - t)^\alpha y \quad z = (t_s - t)^\beta \xi \quad S = (t_s - t)^\alpha f(\xi),$$

$$w = (t_s - t)^\gamma W(t, y, \xi) \quad u = (t_s - t)^{\gamma + \alpha - \beta} U(t, y, \xi) \quad p = (t_s - t)^{-\alpha} P. \qquad (3.3)$$

The expression for u follows from the continuity equation (3.1c) once w is specified, and the scaling for the pressure p is a consequence of the normal stress balance equation (3.1e) since capillary instability drives the dynamics. As before, the geometry of pinching dictates the inequality

$$\alpha > \beta. \qquad (3.4)$$

Consideration of equation (3.1b) for w indicates that if a leading order balance is made between the radial derivative terms of w and the pressure gradient term (this requires $\gamma = \alpha - \beta$), the following *leading order* solution for W arises

$$W = \frac{1}{4} y^2 P_\xi + A(\xi), \qquad (3.5)$$

where $A(\xi)$ is an unknown function. An inconsistency appears now if (3.5) is substituted into the tangential stress balance equation (3.1d). The leading order contribution to (3.1d) after substitution of the scalings (3.3) is simply $W_y = 0$ on $y = f(\xi)$. Application of this condition to the solution (3.5) found above implies that $P_\xi f(\xi) = 0$ leading to an inconsistent solution $P = const.$. A consistent solution is constructed by expanding W (and therefore U) in appropriate powers of $(t_s - t)$ with the leading order contribution of W being independent of y so that the tangential stress balance is satisfied identically to leading order. Higher order corrections from (3.1d) then enter to force a nontrivial solution. The appropriate expansions for w and u become, then,

$$w = (t_s - t)^\gamma \left(W_0(\xi) + (t_s - t)^\beta W_1 + (t_s - t)^\alpha W_2 + \ldots \right), \qquad (3.6a)$$

$$u = (t_s - t)^{\gamma + \alpha - \beta} \left(U_0(y, \xi) + (t_s - t)^\beta U_1 + (t_s - t)^\alpha U_2 + \ldots \right). \qquad (3.6b)$$

The solution for U_0 which is regular at $y = 0$ follows from (3.1c)

$$U_0 = -\frac{1}{2} y W_{0\xi}. \qquad (3.7)$$

Next we obtain the solutions for W_1 and U_1. Using (3.3) and (3.6a) in equation (3.1b) gives

$$(t_s - t)^{\gamma - 2\alpha} \left(\frac{\partial^2}{\partial y^2} + \frac{1}{y} \frac{\partial}{\partial y} \right) \left((t_s - t)^\beta W_1 + (t_s - t)^\alpha W_2 + \ldots \right)$$

$$+ (t_s - t)^{\gamma - 2\beta} W_{0\xi\xi} + \ldots = (t_s - t)^{-\alpha - \beta} P_\xi. \qquad (3.8)$$

10

Balance of the leading order terms involving W_0, W_1 and P gives

$$\alpha = \frac{3}{2}\beta \qquad \gamma = -\frac{1}{2}\beta, \tag{3.9}$$

and a solution for W_1 follows by integration with respect to y since the pressure is independent of y by the normal stress balance (see comments below also)

$$W_1 = \frac{1}{4}y^2(P_\xi - W_{0\xi\xi}) + A(\xi), \tag{3.10}$$

where A is some function of ξ. Using (3.10) and (3.1c) gives

$$U_1 = -\frac{1}{16}y^3(P_{\xi\xi} - W_{0\xi\xi\xi}) + \frac{1}{2}yA_\xi. \tag{3.11}$$

Implicit in the solutions (3.10), (3.11) is the assumption that $P_y = 0$. Using the values (3.9) for α and γ shows that the leading order balance in (3.1a) is

$$\left(\frac{\partial^2}{\partial y^2} + \frac{1}{y}\frac{\partial}{\partial y} - \frac{1}{y^2}\right)U_0 = P_y. \tag{3.12}$$

Now substitution of the solution (3.7) for U_0 into (3.12) shows that the left hand side is zero and so

$$P_y = 0. \tag{3.13}$$

Equation (3.13) is crucial for the consistency of the theory.

Next we consider the tangential stress balance. Using the values (3.9) gives the following equation to leading order

$$U_{0\xi} + W_{1y} + 2U_{0y}f' - 2W_{0\xi}f' = 0 \quad y = f(\xi). \tag{3.14}$$

Use of solutions (3.7) and (3.10) into (3.14) gives an ordinary differential equation for $W_0(\xi)$,

$$\left(f^3 W_0'\right)' = \frac{1}{2}f^3 P'. \tag{3.15}$$

An expression for P in terms of W_0 is available from the normal stress balance equation. It is found that to leading order several terms in this equation are in balance (according to the previously found values (3.9)) the result being

$$P - 2U_{0y} = \frac{1}{f} \quad y = f(\xi).$$

Substitution of this into (3.15) and integration gives the solution

$$W_0' = -\frac{1}{3f} + \frac{k}{f^2}, \tag{3.16}$$

11

where k is a constant of integration. With W_0 known in terms of f, an equation for f arises from the kinematic condition (3.1f) and use of the ansatz (3.3) along with the appropriate derivative transformations (see Section 2 also). To leading order, therefore, the kinematic condition becomes

$$(t_s - t)^{\gamma + \alpha - \beta} U_0 = (t_s - t)^{\alpha - 1}(-\alpha f + \beta \xi f') + (t_s - t)^{\alpha + \gamma - \beta} W_0 f'.$$

A balance of terms is achieved if $\gamma + \alpha - \beta = \alpha - 1$ which along with (3.9) gives

$$\alpha = 1 \qquad \beta = \frac{2}{3} \qquad \gamma = -\frac{1}{3}. \tag{3.17}$$

The kinematic equation is

$$\left(W_0 + \frac{2}{3}\xi\right) f' + \left(-1 + \frac{1}{2}W_0'\right) f = 0,$$

which on elimination of W_0' from (3.16) becomes

$$\left(W_0 + \frac{2}{3}\xi\right) f' + \left(-f - \frac{1}{6} + \frac{k}{2f}\right) = 0. \tag{3.18}$$

Equations (3.16) and (3.18), therefore, provide a coupled system of first order equations to be solved subject to conditions at $\xi = 0$, for instance. In subsections 3.1 and 3.2 that follow we consider analytical and computational aspects of this system.

First, some comments on the consistency of our theory with the original assumption that the flow is in the Stokes regime are necessary. It is seen from the values (3.17) that the axial and radial velocities (see (3.6a,b)) have size $O((t_s - t)^{-1/3})$ and $O(1)$ respectively at the time of pinching. The magnitude of the velocity vector is becoming infinite, therefore, and the possibility of violation of the Stokes flow assumption arises. The terms ignored are the unsteady and convective terms of the Navier-Stokes equations which read

$$R_e(u_t + uu_r + uw_z) = -p_r + \triangle u - \frac{u}{r^2}, \tag{NS1}$$

$$R_e(w_t + uw_r + ww_z) = -p_z + \triangle w, \tag{NS2}$$

where $R_e = \frac{\sigma \rho R}{\mu^2}$ is the Reynolds number. In deriving the similarity equations (3.16), (3.18) we use information from U_0, U_1 in (NS1) and W_0, W_1 in (NS2). The smallest terms considered, therefore, are of $O((t_s - t)^{-4/3})$ in (NS1) and $O((t_s - t)^{-5/3})$ in (NS2), coming from the Laplacian of U_1 and W_1 respectively. The largest possible terms which would enter through the unsteady and convective terms on the left hand side of (NS1) and (NS2) are easily calculated to be of orders $O((t_s - t)^{-1})$ and $O((t_s - t)^{-4/3})$ respectively. As $t \to t_s-$, therefore, the validity of the Stokes approximation and the ansatz leading to (3.16), (3.18) is consistent; higher order terms eventually enter via unsteadiness and nonlinearity in (NS1) and (NS2) but are of no consequence to the leading order balances constructed here.

3.1 Analysis of the similarity equations

Elimination of W_0 between (3.16) and (3.18) yields a single second order equation for f which can be written as:

$$\left(f^2 + \frac{1}{6}f - \frac{k}{2}\right)\frac{d^2f}{d\xi^2} = \left(\frac{f^2 + f - \frac{3k}{2}}{3f}\right)\left(\frac{df}{d\xi}\right)^2 \tag{3.19}$$

At first sight, equation (3.19) appears to admit a class of even solutions which, without loss of generality, may satisfy $f(0) = f_0$, $f'(0) = 0$. A series solution for small ξ, however, with the above initial conditions is found to yield a constant solution $f(\xi) = f_0$. For general values of ξ it can be shown that acceptable solutions to (3.19) produce monotonic functions. Two distinct cases need to be considered, (a) $k \leq 0$, (b) $k > 0$.

We consider the case $k \leq 0$ first. If we assume that f' vanishes at some finite value of $\xi = \xi_0$ say, then by (3.18) we deduce that $W_0'(\xi_0) = 2$. Using this in (3.16), however, requires $-\frac{1}{3f(\xi_0)} + \frac{k}{f^2(\xi_0)} = 2$ which is impossible since $k \leq 0$ and $f(\xi_0) > 0$, showing that f' is non-vanishing and so $f(\xi)$ is monotonic. This result can also be proved by construction of closed form expressions for f'. We integrate (3.19) once with respect to ξ so that

$$\frac{df}{d\xi} = AG(f),$$

$$\frac{\partial}{\partial f}(ln(G(f))) = \frac{f^2 + f - \frac{3}{2}k}{3f(f^2 + \frac{1}{6}f - \frac{k}{2})}, \tag{3.20}$$

where A is a constant. Equation (3.20) can be integrated explicitly. There are three distinct cases: (i) $k = 0$, (ii) $k < -\frac{1}{72}$, (iii) $-\frac{1}{72} < k < 0$, giving the following solutions.

Case (i), $k = 0$

$$G(f) = \frac{f^2}{(f + 1/6)^{\frac{5}{3}}}. \tag{3.21a}$$

Case (ii). $k < -1/72 \; (k = -2\lambda^2)$

$$G(f) = \frac{f}{(f^2 + \frac{1}{6}f + \lambda^2)^{\frac{1}{3}}} \exp\left(\frac{2}{9\sqrt{\lambda^2 - \frac{1}{144}}}\tan^{-1}\left(\frac{f + \frac{1}{12}}{\sqrt{\lambda^2 - \frac{1}{144}}}\right)\right). \tag{3.21b}$$

Case (iii), $-1/72 < k < 0 \; (\mu = (\frac{k}{2} + \frac{1}{144})^{1/2})$

$$G(f) = f(f + \frac{1}{12} + \mu)^{-\frac{1}{3} - \frac{1}{9\mu}}(f + \frac{1}{12} - \mu)^{-\frac{1}{3} + \frac{1}{9\mu}}. \tag{3.21c}$$

These expressions show that $G(f)$, and hence f', is non-vanishing; cases (i) and (ii) are straightforward while in case (iii) the observation $|\mu| < \frac{1}{12}$ yields the desired conclusion.

13

When $k > 0$ the expression for G is identical to (3.21c) with μ as given there. It follows that for $k > 0$,

$$\frac{1}{12} < \mu < \infty,$$

with equality on the lower bound already covered by the case $k = 0$ in (3.21a). Using this inequality we see from (3.21c) that at positions where $f = \mu - \frac{1}{12}$, the derivative f' can (i) become infinite, (ii) be finite and non-zero, (iii) become zero, depending on the value of the exponent $-\frac{1}{3} + \frac{1}{9\mu}$. In terms of μ these three cases are

$$\mu > \frac{1}{3} \quad , \quad \mu = \frac{1}{3} \quad , \quad \mu < \frac{1}{3},$$

respectively. In what follows we show (by sketching the behavior rather than presenting rigorous proofs) that case (ii) alone allows admissible solutions.

We consider the range $\frac{1}{3} < \mu < \infty$ first. As mentioned above the slope f' becomes infinite at positions ξ_0 given implicitly by $f(\xi_0) = \mu - \frac{1}{12}$. The interfacial slope becomes double valued; a local analysis in the vicinity of $f_0 = \mu - \frac{1}{12}$ gives

$$\xi - \xi_0 \sim (f - f_0)^q \qquad \frac{2}{3} < q < 2.$$

We note that an infinite slope in f violates the ansatz established by the scalings (3.17) since spatial variations in the axial direction become much larger than the variation in the radial direction.

Next, we consider the values $\frac{1}{12} < \mu < \frac{1}{3}$. It is seen from (3.21c) that the derivative vanishes when $f = \frac{1}{12} - \mu$ since the exponent of the last factor satisfies $0 < -\frac{1}{3} + \frac{1}{9\mu} < 1$. This inequality for the exponent, however, implies that higher derivatives of the interfacial amplitude in the similarity region are unbounded and this case is dropped since we are interested in smooth solutions.

The final possibility is $\mu = \frac{1}{3}$ $(k = \frac{5}{24})$ which casts (3.21c) into

$$G(f) = f(f + \frac{5}{12})^{-\frac{2}{3}}. \tag{3.21d}$$

Equations (3.21a) and (3.21d) can be integrated to yield closed form expressions for ξ in terms of f; the solutions for f are implicit, therefore, and are not very illuminating besides the checks they provide for the numerical and asymptotic work. These solutions are

$k = 0,$ (3.21a)

$$-\frac{(f + \frac{1}{6})^{\frac{5}{3}}}{f} + \frac{5}{3}I(f; \frac{1}{6^{1/3}}) = A_0\xi + B_0, \tag{3.22a}$$

$k = \frac{1}{3},$ (3.21d)

14

$$I(f; \frac{5^{1/3}}{12^{1/3}}) = A_1\xi + B_1, \qquad (3.22b)$$

where

$$I(f;\kappa) = \frac{3}{2}(f + \kappa^3)^{\frac{2}{3}} + \kappa^2 ln\left((f + \kappa^3)^{\frac{1}{3}} - \kappa\right)$$

$$-\kappa^2 ln\left((f + \kappa^3)^{\frac{2}{3}} + \kappa(f + \kappa^3)^{\frac{1}{3}} + \kappa^2\right) + \frac{4\kappa^2}{\sqrt{3}}\tan^{-1}\left(\frac{2(f + \kappa^3)^{\frac{1}{3}} + \kappa}{\kappa\sqrt{3}}\right).$$

The constants A_0, A_1, B_0, B_1 are found from the initial conditions on f and f' at $\xi = 0$ for instance. The behavior of the solutions (3.22a,b) for large $|\xi|$ are easily obtainable. Without loss of generality we assume $A_{0,1} > 0$ to obtain

$\underline{k = 0}$

$$f \sim \left(\frac{2A_0}{3}\right)^{3/2} \xi^{3/2} \quad \xi \to \infty,$$

$$f \sim -\frac{1}{6^{\frac{5}{3}}}\frac{1}{\xi} \quad \xi \to -\infty. \qquad (3.23a, b)$$

$\underline{k = \frac{1}{3}}$

$$f \sim \left(\frac{2A_0}{3}\right)^{3/2} \xi^{3/2} \quad \xi \to \infty,$$

$$f \sim \exp(\frac{A_1 12^{1/3}}{5^{1/3}}\xi) \quad \xi \to -\infty. \qquad (3.24a, b)$$

For general values of k the asymptotic behavior is more easily obtainable directly from equation (3.19). Assuming that $f'(0) > 0$, we look for solutions that grow as $\xi \to +\infty$ but decay as $\xi \to -\infty$ (such behavior is supported by the closed form solutions (3.22a,b) as well as numerical calculations). To leading order, equation (3.19) takes the forms

$$\frac{f''}{f'} = \frac{1}{2}\frac{f'}{f} \quad f \gg 1, \qquad (3.25a)$$

$$\frac{f''}{f'} = \frac{f'}{f} \ (k \neq 0) \quad , \quad \frac{f''}{f'} = 2\frac{f'}{f} \ (k = 0) \quad f \ll 1. \qquad (3.25b, c)$$

It can be seen that for large positive ξ the asymptotic form is independent of k, in agreement with (3.23a) (3.24a) above. The asymptotic forms are, therefore,

$$f \sim \xi^{3/2} \quad \xi \to \infty, \qquad (3.26a)$$

$$f \sim \exp(-q|\xi|) \ (k \neq 0) \quad f \sim |\xi|^{-1} \ (k = 0) \quad \xi \to -\infty, \qquad (3.26b)$$

where q is a positive constant which can be determined numerically. Given the behavior of f the asymptotic forms for the axial jet velocity W_0 follow from equation (3.16),

$$W_0 \sim const. + O(\xi^{-1/2}) \quad \xi \to \infty, \qquad (3.27a)$$

$$W_0 \sim \exp(2q|\xi|) \quad (k \neq 0) \qquad W_0 \sim |\xi|^3 \quad (k = 0) \qquad \xi \to -\infty. \qquad (3.27b)$$

In the following section we present numerical solutions of the similarity equations with particular emphasis on the verification of the analytical findings of this section.

3.2   Numerical solutions of the similarity equations

Equations (3.16), (3.18) or equivalently equation (3.19) were solved numerically by specifying conditions at $\xi = 0$ and integrating out to $+\infty$ and $-\infty$. Typically we worked with the second order equation (3.19) with initial conditions $f(0) = f_0$ and $f'(0) = f_1 > 0$. Integration to an appropriately large positive and negative value of ξ was achieved by a fourth order Runge-Kutta method. Representative solutions are considered for the three cases (i) $k < 0$, (ii) $k = 0$, (iii) $k = \frac{1}{3}$. We note that the distinctions between different negative values of k are not important in the numerical calculations.

Figure 9 shows the results for f and W_0 of a case having $k = -1$ and initial conditions $f(0) = 1$ and $f'(0) = 1$. To establish the asymptotic behavior of the solutions for large $|\xi|$ we construct logarithmic plots of the relevant parts of the solutions. Results for large negative ξ are shown in Figure 10 which shows the variation of $ln(f)$ and $ln(w)$ with ξ. The computed slopes included on the curves were calculated by a least squares fitting of the data. According to the asymptotic forms (3.26b) and (3.27b), w grows exponentially at twice the rate at which f decays exponentially. The computed slopes of 2.269 and -1.138 for $ln(w)$ and $ln(f)$ respectively are in full agreement with this finding. The asymptotic form (3.26a) for large positive ξ is confirmed in Figure 11 with very good agreement. Verification of the behavior of W_0 was also obtained by plotting the variation of W_0 with $\xi^{-1/2}$ for large ξ.

For $k = 0$ and the same initial conditions as above qualitatively similar solutions are obtained for both f and W_0 and representative solutions are given in Figure 12. A comparison between the numerical and asymptotic solutions for large positive ξ according to (3.23a) is described next. The behavior (3.23a) is equivalent to

$$ln(f) \sim \frac{3}{2} ln\left(\frac{2}{3}\right) + \frac{5}{2} ln\left(\frac{7}{6}\right) + \frac{3}{2} ln(\xi).$$

The value of the intercept follows from (3.20) when the values $f(0) = f'(0) = 1$ are used, and is equal to -0.224. A logarithmic plot of the numerical solution produced a slope of 1.498 and an intercept -0.208 (these results were obtained by integration to $\xi = 500$; these values improve as the maximum integration range is increased). The results for $k = \frac{1}{3}$ are qualitatively similar to those described above and are not included here.

16

4 Conclusions

A formal theory has been developed to describe the breakup process of highly viscous or inviscid jets in air. The similarity solutions obtained here constitute inner solutions in the vicinity of regions where the jet radius is going to zero which when matched with outer solutions of the Stokes or Euler equations respectively, provide a full description of the breakup phenomenon. In general the outer solutions are fully nonlinear and must be computed numerically. In numerical calculations of jet breakup (by boundary integral methods for example), it is important to have a rational way of continuing the computations beyond the change in topology necessitated by the physics. The similarity solutions presented here provide such a possibility since accurate initial conditions for the pinched part of the evolution, consistent with the full equations of motion can be easily calculated. Direct simulations near the pinching times contain stiffness problems which are likely to produce inaccuracies. Another example of the need of accurate initial conditions for the jet evolution beyond breakup is the experimentally and computationally observed behavior of a residual fluid tube at breakup being accelerated by surface tension to form a jet which can go through the mother drop it was connected to. The speeds of such jets depend on interfacial tension forces which are proportional to the interfacial surface area and hence the shape at breakup.

As an illustration of the mechanics of the matching process we consider the results of Section 3 for highly viscous jets. Matching is achieved as $|\xi| \to \infty$ and so the asymptotic forms of the solutions are essential in achieving this. Using (3.26a), for example, we have $f \sim \xi^{3/2}$ as $\xi \to \infty$. Changing to physical (outer) variables using the ansatz (3.3) and the scales (3.17) gives the following condition to be satisfied by the outer solution as $z \to 0$ (we have assumed, without loss of generality that pinching occurs at $z = 0$),

$$S \sim z^{\frac{3}{2}}.$$

The multiplicative constant that goes along with this behavior and which can be found from the outer solution, fixes the inner problem whose solution is easily obtained from the similarity equations.

We have also found a qualitative difference between the breakup forms of inviscid jets with surface tension and their highly viscous counterparts. In the former case our solutions indicate that at breakup the interface is more or less symmetric with growth to mother drops on either side of the pinch point. In the latter flows (as well as inviscid jets with zero surface tension), our similarity solutions indicate that at breakup there are thin, and relatively long, fluid tubes which taper to zero diameter on one side and grow to connect to a mother drop on the other side. These findings are in full qualitative agreement with photographs from

17

various experiments on both highly viscous jets (Tjahjadi et al. 1992) as well as inviscid ones (Donnelly and Glaberson 1966, Chaudhary and Maxworthy 1980a,b).

REFERENCES

- Bogy, D.B. 1979 Drop formation in a circular liquid jet. *Ann. Rev. Fluid Mech.*, **11**, 207-228.

- Chandrasekhar, S. 1961 Hydrodynamic and hydromagnetic stability. Oxford: Clarendon Press.

- Chaudhary, K.C. and Maxworthy, T. 1980a The nonlinear capillary instability of a liquid jet. Part 2. Experiments on jet behavior before droplet formation. *J. Fluid Mech.*, **96**, 275-286.

- Chaudhary, K.C. and Maxworthy, T. 1980b The nonlinear capillary instability of a liquid jet. Part 3. Experiments on satellite drop formation and control. *J. Fluid Mech.*, **96**, 287-297.

- Chaudhary, K.C. and Redekopp, L.G. 1980 The nonlinear capillary instability of a liquid jet. Part 1. Theory. *J. Fluid Mech.*, **96**, 257-274.

- Donnelly, R.J. and Glaberson, W. 1966 Experiments on the capillary instability of a liquid jet. *Proc. Roy. Soc. Lond.*, **A290**, 547-556.

- Drazin, P.G. and Reid, W.H. 1981 Hydrodynamic stability. Cambridge University Press.

- Goedde, E.F. and Yuen, M.C. 1970 Experiments on liquid jet instability. *J. Fluid Mech.*, **40**, 495-511.

- Mansour, N. and Lundgren, T.S. 1990 Satellite formation in capillary jet breakup. *Phys. Fluids A*, **2**, 1141-1144.

- Papageorgiou, D.T. and Orellana, O. 1993 Pinching solutions of slender cylindrical jets. Submitted to *SIAM J. Appl. Math.*.

- Rayleigh, Lord 1878 On the instability of jets. *Proc. Lond. Math. Soc.*, **10**, 4-13.

- Stuart, J.T. 1960 On the nonlinear mechanics of wave disturbances in stable and unstable parallel flows. Part 1. The besic behavior in plane Poiseuille flow. *J. Fluid Mech.*, **9**, 353-370.

- Ting, L. and Keller, J.B. 1990 Slender jets and thin sheets with surface tension. *SIAM J. Appl. Math.*, **50** No. 6, 1533-1546.

- Tjahjadi, M., Stone, H.A. and Ottino, J.M. 1992 Satellite and subsatellite formation in capillary breakup. *J. Fluid Mech.*, **243**, 297-317.

- Tomotika, S. 1935 On the stability of a cylindrical thread of a viscous liquid surrounded by another viscous fluid. *Proc. Roy. Soc. Lond.*, **A150**, 322-337.

- Watson, J. 1960 On the nonlinear mechanics of wave disturbances in stable and unstable parallel flows. Part 2. The development of a solution for plane Poiseuille flow and plane Couette flow. *J. Fluid Mech.*, **9**, 371-389.

- Yuen, M.-C. 1968 Nonlinear capillary instability of a liquid jet. *J. Fluid Mech.*, **33**, 151-163.

Zero surface tension (inviscid)
f(0)=1 g(0)=1 beta=4/7
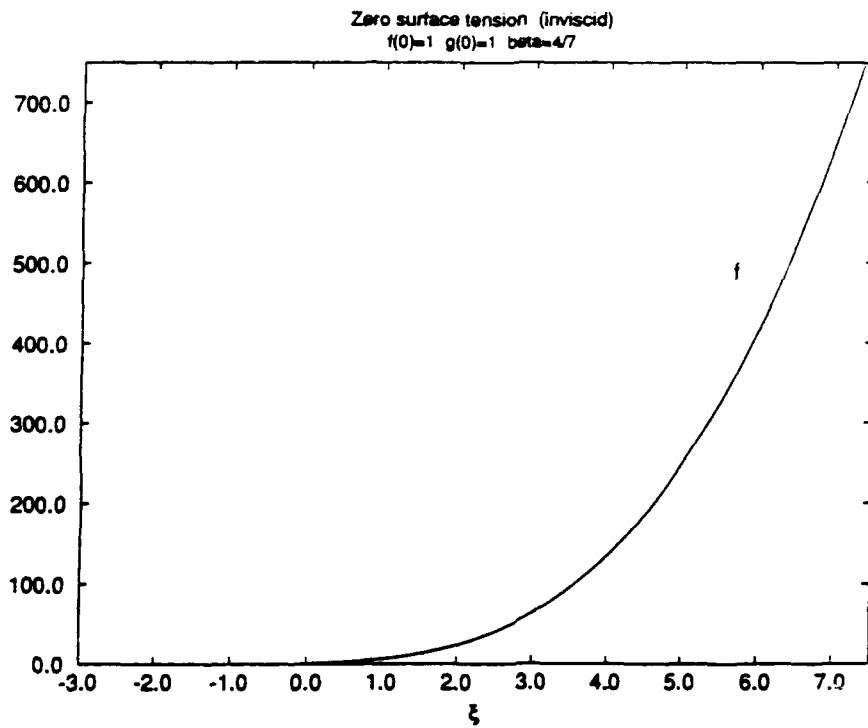
• **Figure 1** Inviscid jet with zero surface tension; similarity solution $f(\xi)$.

Zero surface tension (inviscid)
f(0)=1 g(0)=1 beta=4/7
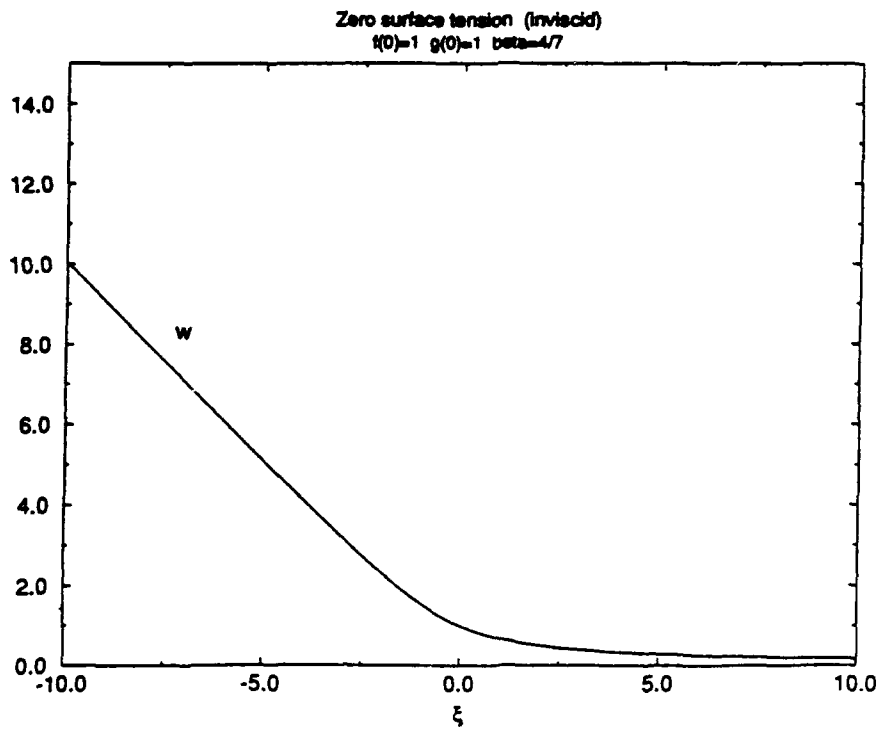
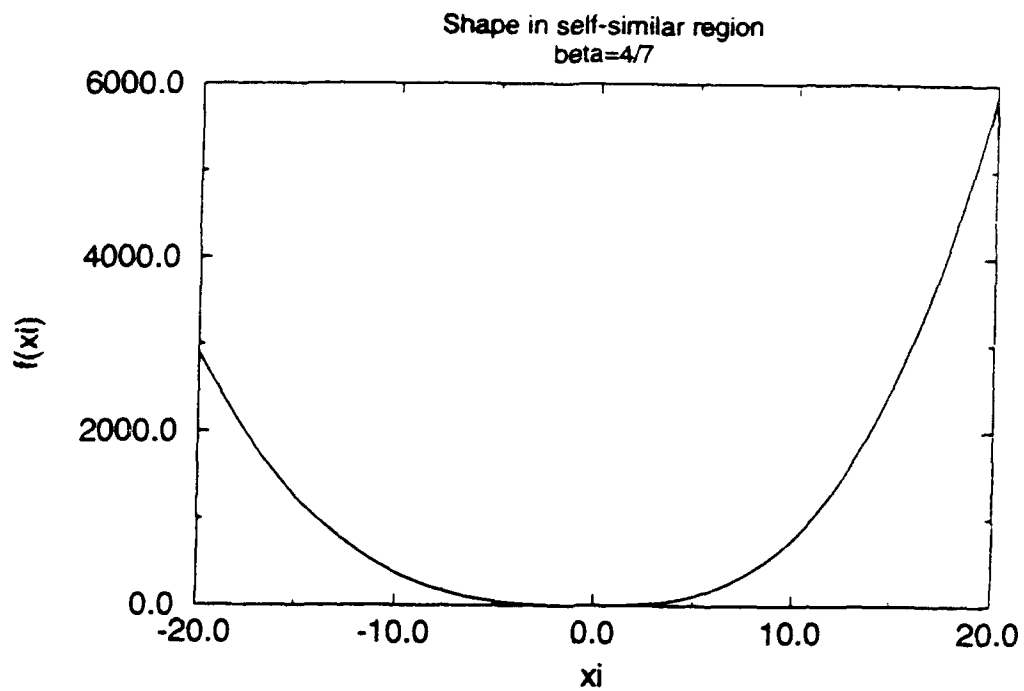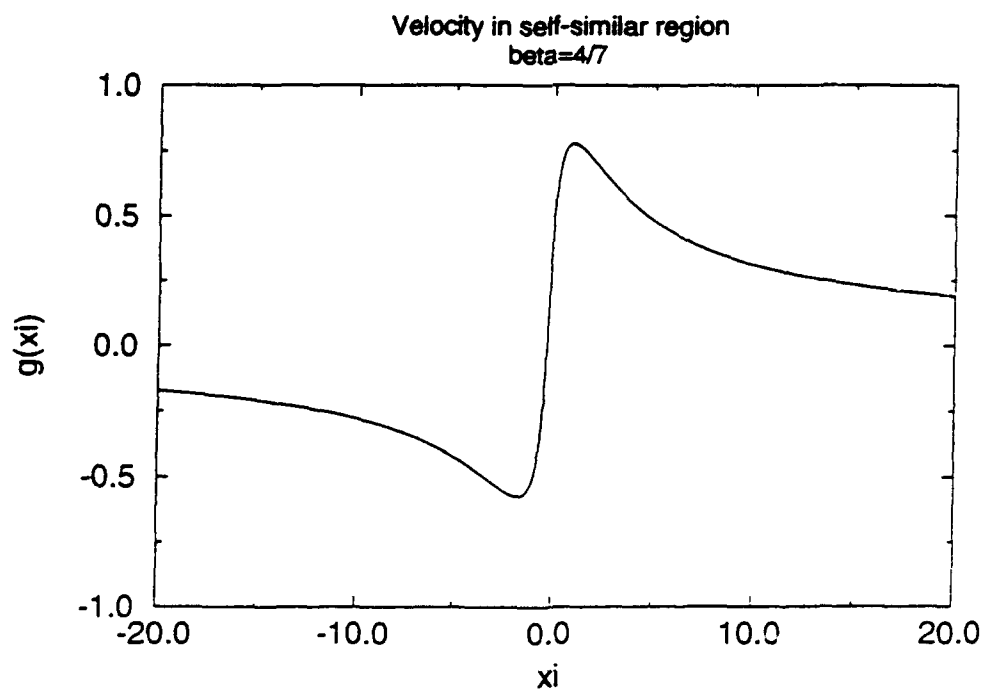• **Figure 2** Inviscid jet with zero surface tension; similarity solution $g(\xi)$.

21
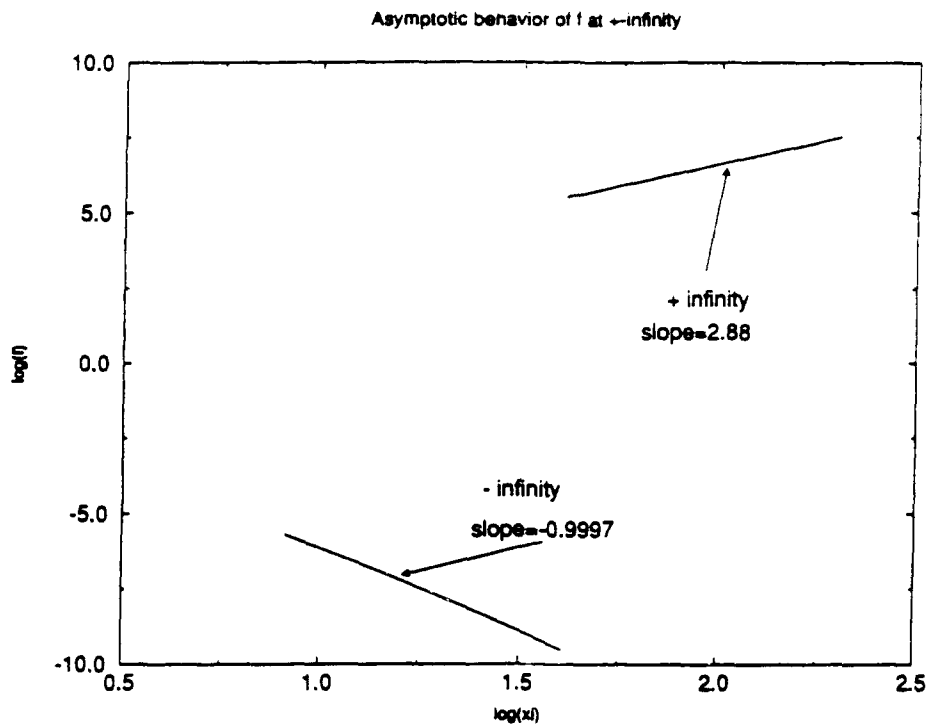
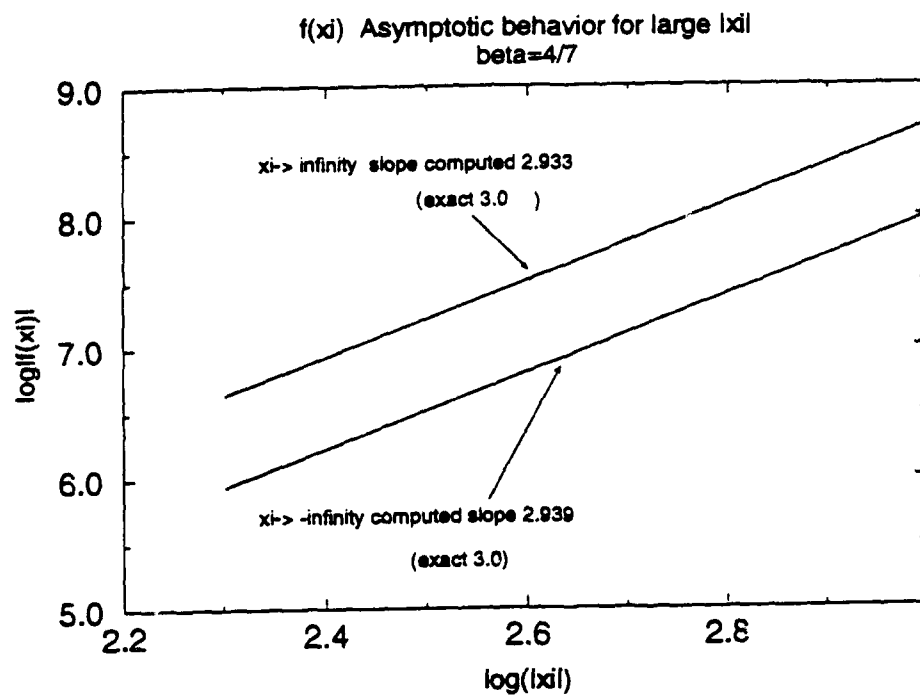**Figure 3** Inviscid jet with zero surface tension; asymptotic behavior of $f(\xi)$.
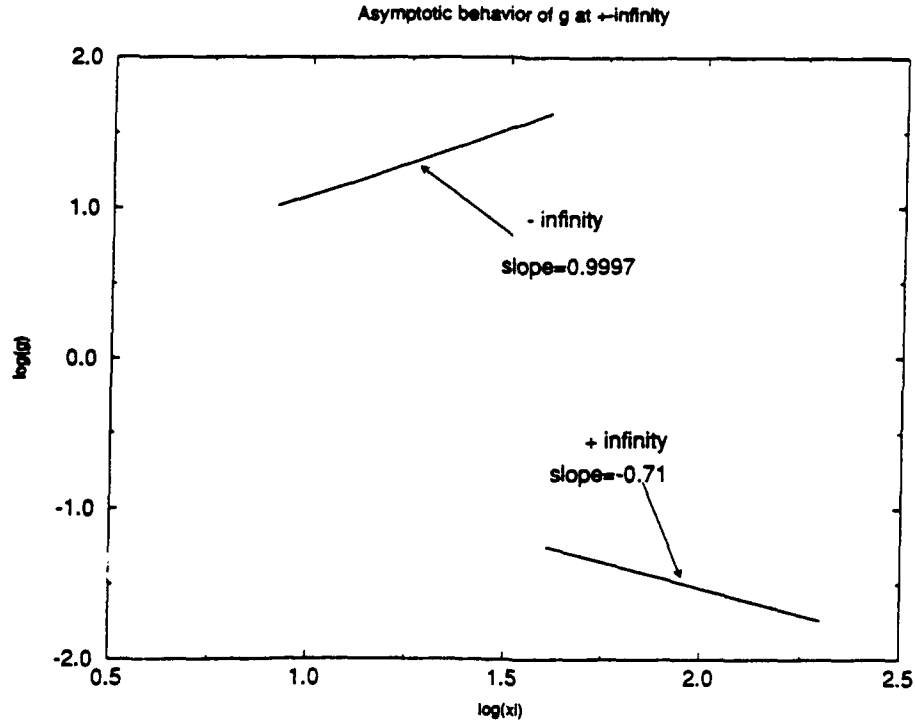
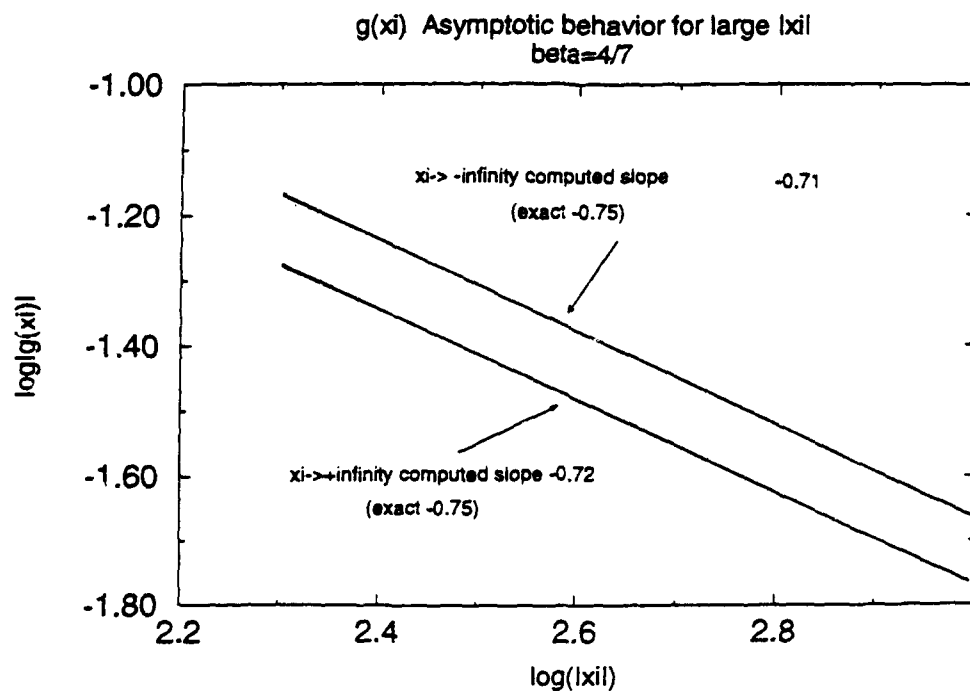**Figure 4** Inviscid jet with zero surface tension; asymptotic behavior of $g(\xi)$.

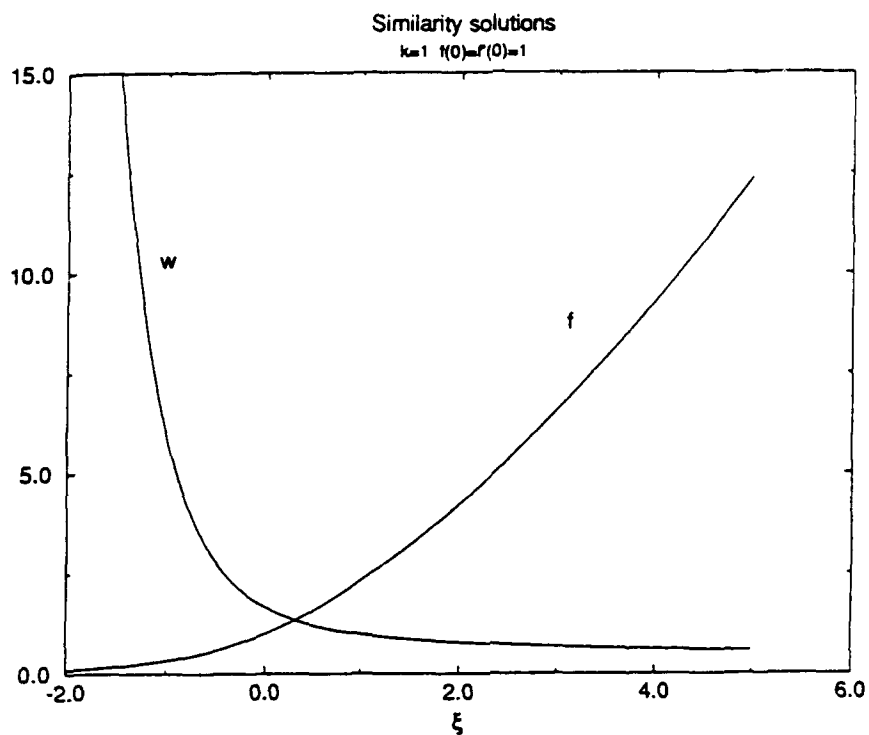• **Figure 5** Inviscid jet with surface tension; similarity solution $f(\xi)$.

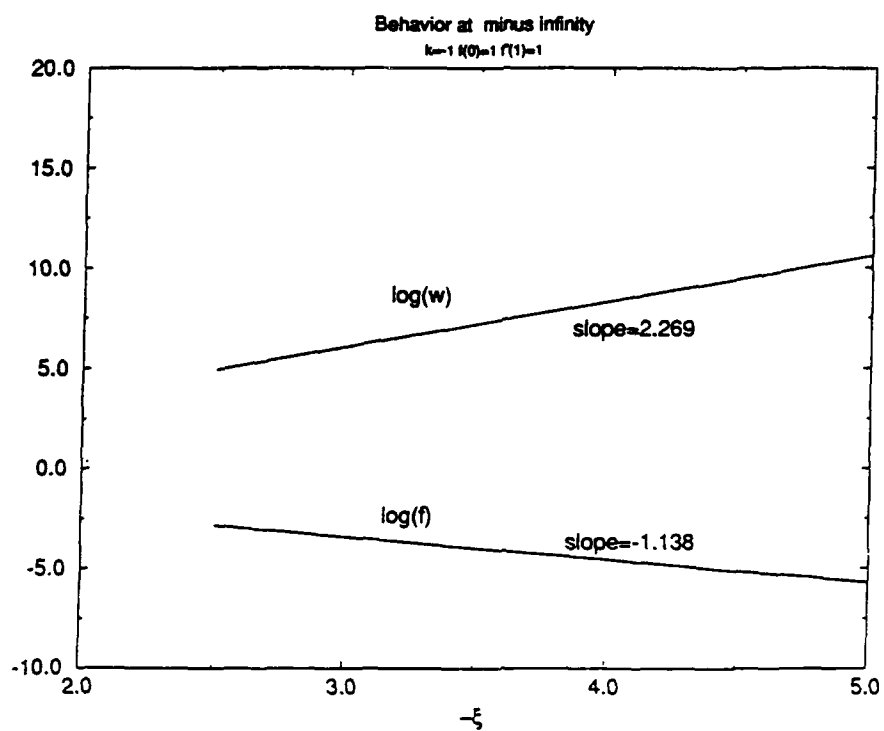• **Figure 6** Inviscid jet with surface tension; similarity solution $g(\xi)$.

23

• **Figure 7** Inviscid jet with surface tension; asymptotic behavior of $f(\xi)$.
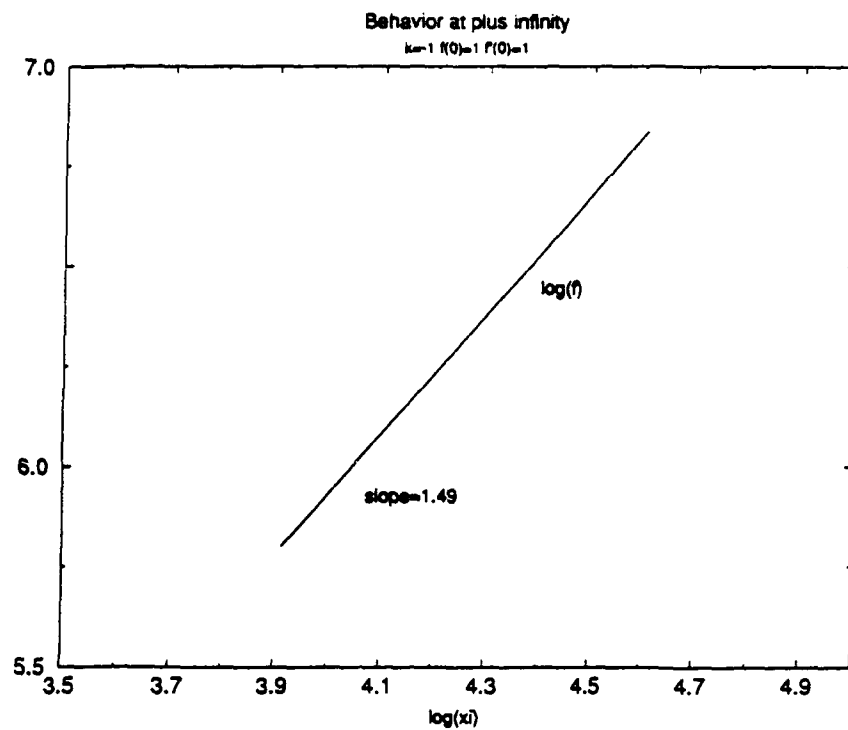

• **Figure 8** Inviscid jet with surface tension; asymptotic behavior of $g(\xi)$.

24

- **Figure 9** Highly viscous jet with surface tension. Similarity solutions $W_0(\xi)$ $f(\xi)$. $k = -1$, initial conditions $f(0) = 1$, $f'(0) = 1$.

- **Figure 10** Highly viscous jet with surface tension. Asymptotic behavior as $\xi \to +\infty$. $k = -1$, initial conditions $f(0) = 1$, $f'(0) = 1$.

25

Behavior at plus infinity
k=-1 f(0)=1 f'(0)=1

log(f)

slope=1.49

log(xi)

- **Figure 11** Highly viscous jet with surface tension. Asymptotic behavior as $\xi \to -\infty$. $k = -1$, initial conditions $f(0) = 1$, $f'(0) = 1$.
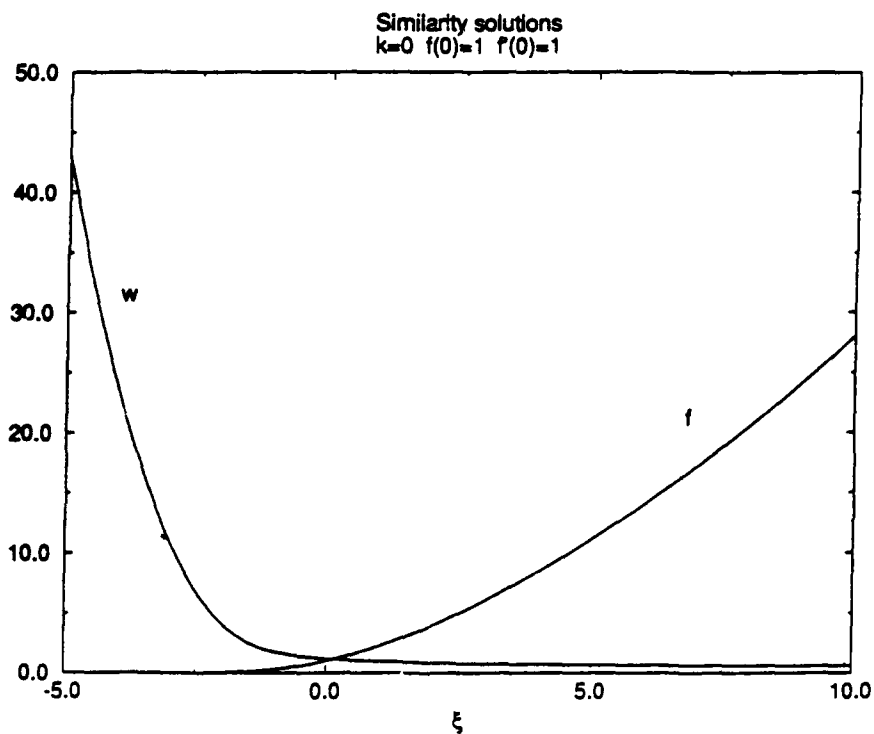

Similarity solutions
k=0 f(0)=1 f'(0)=1

w

f

ξ

- **Figure 12** Highly viscous jet with surface tension. Similarity solutions $W_0(\xi)$ $f(\xi)$. $k = 0$, initial conditions $f(0) = 1$, $f'(0) = 1$.

26

REPORT DOCUMENTATION PAGE

Public reporting burden for this collection of information is estimated to average 1 hour per response, including the time for reviewing instructions, searching existing data sources, gathering and maintaining the data needed, and completing and reviewing the collection of information. Send comments regarding this burden estimate or any other aspect of this collection of information, including suggestions for reducing this burden, to Washington Headquarters Services, Directorate for Information Operations and Reports, 1215 Jefferson Davis Highway, Suite 1204, Arlington, VA 22202-4302, and to the Office of Management and Budget, Paperwork Reduction Project (0704-0188), Washington, DC 20503.

1. AGENCY USE ONLY (Leave blank)	2. REPORT DATE July 1993	3. REPORT TYPE AND DATES COVERED Contractor Report

4. TITLE AND SUBTITLE	5. FUNDING NUMBERS
ANALYTICAL DESCRIPTION OF THE BREAKUP OF LIQUID JETS IN AIR	C NAS1-19480
6. AUTHOR(S) Demetrios T. Papageorgiou	WU 505-90-52-01

7. PERFORMING ORGANIZATION NAME(S) AND ADDRESS(ES) Institute for Computer Applications in Science and Engineering Mail Stop 132C, NASA Langley Research Center Hampton, VA 23681-0001	8. PERFORMING ORGANIZATION REPORT NUMBER ICASE Report No. 93-45

9. SPONSORING/MONITORING AGENCY NAME(S) AND ADDRESS(ES) National Aeronautics and Space Administration Langley Research Center Hampton, VA 23681-0001	10. SPONSORING/MONITORING AGENCY REPORT NUMBER NASA CR-191503 ICASE Report No. 93-45

11. SUPPLEMENTARY NOTES

Langley Technical Monitor: Michael F. Card   Submitted to Journal
Final Report   of Fluid Mechanics

12a. DISTRIBUTION/AVAILABILITY STATEMENT Unclassified – Unlimited Subject Category 34	12b. DISTRIBUTION CODE

13. ABSTRACT (Maximum 200 words)

A viscous or inviscid cylindrical jet with surface tension in a vacuum tends to pinch due to the mechanism of capillary instability. We construct similarity solutions which describe this phenomenon as a critical time is encountered, for two physically distinct cases: (i) Inviscid jets governed by the Euler equations, (ii) highly viscous jets governed by the Stokes equations. In both cases the only assumption imposed is that at the time of pinching the jet shape has a radial length scale which is smaller than the axial length scale. For the inviscid case, we show that our solution corresponds exactly to one member of the one-parameter family of solutions obtained from slender jet theories and the shape of the jet is locally concave at breakup. For highly viscous jets our theory predicts local shapes which are monotonic increasing or decreasing indicating the formation of a mother drop connected to the jet by a thin fluid tube. This qualitative behavior is in complete agreement with both direct numerical simulations and experimental observations.

14. SUBJECT TERMS nonlinear solutions, singularity formation	15. NUMBER OF PAGES 30
	16. PRICE CODE A03

17. SECURITY CLASSIFICATION OF REPORT Unclassified	18. SECURITY CLASSIFICATION OF THIS PAGE Unclassified	19. SECURITY CLASSIFICATION OF ABSTRACT	20. LIMITATION OF ABSTRACT